Tunable RF MEMS and Its Applications

Zewen Liu, Huiliang Liu, Julien Sarrazin

Tunable RF MEMS and Its Applications

Zewen Liu[a], Huiliang Liu[a], and Julien Sarrazin[b]

[a] Institute of Microelectronics, Tsinghua University, Beijing 100084, CHINA
[b] Electronics & Electromagnetism Laboratory, University of Pierre & Marie Curie, Paris 75252, FRANCE

With fast development of mobile communication technology, the increasingly complex communicating environment and the crowded spectrum have raised stringent requirements on the RF front-end performance. In this paper, the influence of human body on the communication performance is analyzed. In particular, it is shown that the antenna input impedance faces huge variation in the frame of body-centric devices. Consequently, automatic impedance matching appears to be crucial to improve the performance withstand the inconstant environment. The investigation of key tunable components of RF MEMS is therefore presented. A variable capacitor with symmetric balanced structure is designed to achieve a large capacitance tuning ratio and a remarkable linearity of the C-V response. The proposed RF MEMS variable capacitor was modeled and simulated. The results show a linearity factor of 99.82% in C-V response and a large tuning ratio of 480% in a low actuation voltage range from 0V to 16.3V.

Introduction

With fast development of wireless communication technology, the growth in the number of mobile users has been explosive. Besides the requirement of voice communication, the growth of the usage of mobile internet and multi-media services are still far from saturation (1), which also drives the demand for higher data rates. The mobile terminals continue to develop to multi-mode multi-band devices at a rapid pace (2). For example the 3GPP release 11 standard has twenty RF bands (3). The realization of multi-band multi-mode device needs to be supported by reducing form factor, complexity and BOM count of modules (4), which cause stringent requirements on design. Tunable RF MEMS supplies possible solution to make the front-end modules reconfigurable for different bands and modes to meet the space limitation with reduction of the component number (5, 6). The greater effect of human body on multi-band multi-mode device is another reason to make the front-end tunable. The detail influence of human body on the communication performance is analyzed in next section, by considering the characteristics of propagation in close proximity of the human body. From this study, the need of automatic impedance matching networks is highlighted. To meet the requirement of such applications, tunable RF MEMS components are considered in this paper. With its advantage of low loss, high Q-factor and high linearity, the excellent electrical performance of RF MEMS tunable capacitors determines the good selectivity and linearity. Several typical structures of RF MEMS variable capacitors are investigated. The design of a symmetric balanced structured MEMS varactor, with flexible upper plate of the capacitor moves upwards

when the voltage added on the control electrodes increases, presents a highly linear decrease of the capacitance with increasing control voltage.

Effect of human body

In addition to the consideration of integration, the effect of human body on multi-band multi-mode device is another reason to make the front-end tunable. The increasingly complex communicating environment with the instantaneous change of human effect has raised more stringent requirements on the RF front-end performance, especially on the antenna behavior. Two main sorts of degradation can be caused by the operator's gesture. One is the increase of absorption, the other is the increase of detuning or impedance mismatching. The increase of user interaction would cause a change in the antenna driving point impedance, as the antenna becoming more resistive and inductive (7). In the frame of Body Area Networks (BAN), where multiple sensors are embedded on the human body or in the clothes, this issue is even more critical. Depending on the human posture or on the space between the cloth and the skin, the environment surrounding the antenna changes drastically. This has an effect on the near-field distribution of the antenna, thereby modifying its input impedance over time.

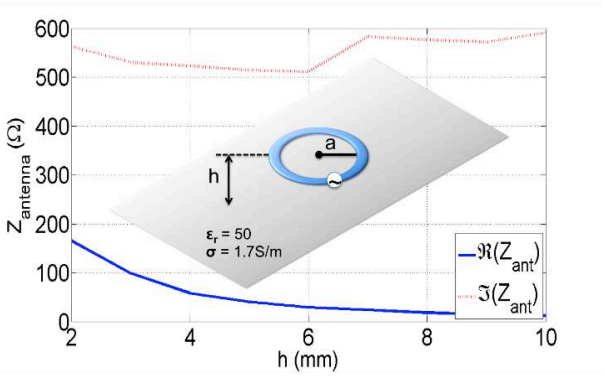

Figure 1. Antenna input impedance variation above human tissue

Consequently, in order to increase antenna efficiency in all flexible conditions, an impedance matching network needs to be considered. To get an idea of the range of variation that the input impedance of an antenna can face in close proximity of the human body, a miniaturized loop antenna (so non-resonant) has been simulated over human tissue at 2.45 GHz with CST Microwave Studio. As a first approximation, the tissue is supposed homogeneous and has a relative permittivity of ε_r=50 and a conductivity of σ=1.7S/m (8). The radius of the loop is a= 7 mm and the distance between the loop and the human tissue is *h*. Antenna input impedance results are shown in Figure 1 over the distance *h*. It can be noticed that the variation cannot be neglected and the real part of the impedance decreases from 165Ω down to 12.2Ω as the distance *h* between the antenna and the human tissue increases. The imaginary part does not follow a constant increase or decrease and is consequently less predictable. It faces a variation of 14% about its mean value.

These results highlight the need of automatic matching impedance circuits for devices operating in close vicinity of human body. Networks capable of matching a wide range of impedance values use tunable capacitors (9). Furthermore, the power consumption of such matching networks should be kept as low as possible. Consequently, RF MEMS

technology appears to be a good candidate as it can provide variable capacitors with low-loss, high linearity and low power consumption.

Tunable RF MEMS Components

The development of RF MEMS switches, capacitors and the integration of these elements into tunable filters, phase shifters and matching networks has been extensively investigated (10). Both switched and voltage controlled variable capacitors can be used as a tuner in RF front end (11). A good example of the switched capacitor has been developed within a mass production capable HV RF CMOS process (12). These RF MEMS capacitors are grouped in flip-chip cells that exhibit a high quality factor of 87 at 2 GHz and operate using a 3.3V supply voltage. The tuning ratio of on-state and off-state is almost 10:1. As it only has two steady state, the switched capacitor can be used in switchable array to form a digital tunable capacitor (13). Compared to switched capacitor, RF MEMS variable capacitor can be tuned continuously with precise capacitance control within the tuning range. But one challenge is the nonlinear C-V response of the common parallel-plate MEMS varactor. The capacitance value changes faster near the pull down point (10), which makes the capacitor more sensitive to the little change of control voltage. To avoid the pull-down effect and enhance the capacitance change range with high linear, a Non-Planar Up-plate and Side Leverage Electrode RF MEMS capacitor (NPUSLE capacitor) is proposed in this paper.

Variable Capacitors

The schematic structure of the proposed variable capacitor is shown in Figure 2. The variable capacitor consists of a movable upper plate and a fixed bottom plate. The symmetric balanced leverage structure controls the movement of the upper plate. Two additional non-plane step structures connected to the upper plate result in a decrese of the initial gap of the capacitor to increase the incipient capacitance value and also lead to a reduction of the upper plate deformation to release the stress. Electrostatic force emerges and makes the upper plate of the capacitor moves upward when control voltage is added. The increasing gap between the upper and bottom plates results in the reduction of capacitance value. The change rate of the plate displacement increases as the control voltage increasing while the change rate of the capacitance value decreases. Therefore, the counteraction of these two change rate leads to a high linearity of the C-V response. As the initial capacitance value is optimized by the non-planar step structure, a variable capacitor can be achieved with a large capacitance tuning ratio and linear C-V response.

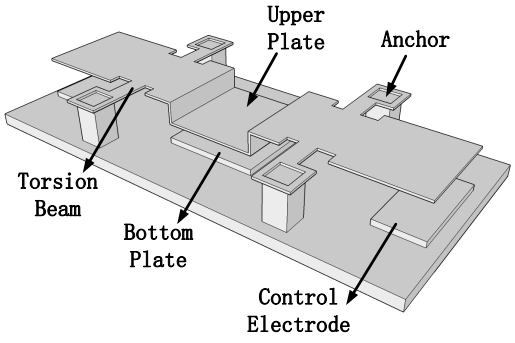

Figure 2. The 3-D structure of the variable capacitor

Figure 3 shows the cross-section of half of the symmetric capacitor structure. When V is added to the control electrode, an electrostatic torque M_e emerges. Then the deformation of the torsion beams generate the restoring torque M_t. An equilibrium will be reached when the two torques are equal as [1] where K_t is the torsional spring constant of the torsion beam and a is the rotation angle of the lever beam. The electrostatic torque M_e can be expressed as [2] (14) where ε_0 is the permittivity of air, A_e is the area of the control electrode and the other geometrical parameters are shown in Figure 3.

$$M_{\mathrm{e}} = M_t = K_t \cdot a \tag{1}$$

$$M_{\mathrm{e}} = \frac{\varepsilon_0 V^2 A_e}{2a^2 l_3}\left[\frac{g_0}{g_0 - l_1 a} - \frac{g_0}{g_0 - l_4 a} + \ln\left(\frac{g_0 - l_1 a}{g_0 - l_4 a}\right)\right] \tag{2}$$

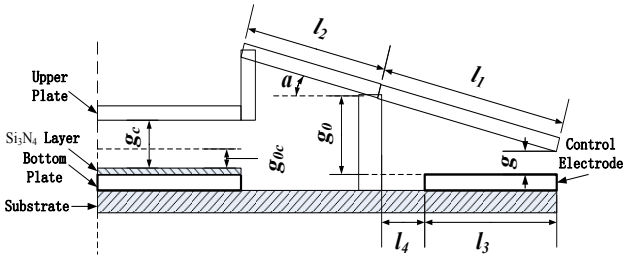

Figure 3. Cross-section of half part of the symmetric capacitor

The torsional spring constant K_t can be calculated as [3] (15) Where l_t, w_t and t_t represent the length, width and thickness of the torsion beam, respectively. G is the shear modulus of the torsion beam, which is 27 GPa for gold. The the expression of the control voltage V can be derived from the equation [1] as [4].

$$K_t = \frac{G w_t t_t^3}{8 l_t}\left[\frac{16}{3} - 3.36\frac{t_t}{w_t}\left(1 - \frac{t_t^4}{12 w_t^4}\right)\right] \tag{3}$$

$$V = \sqrt{\frac{2K_t l_3 a^3}{\varepsilon_0 A_e}\frac{1}{\dfrac{g_0}{g_0 - l_1 a} - \dfrac{g_0}{g_0 - l_4 a} + \ln\dfrac{g_0 - l_1 a}{g_0 - l_4 a}}} \tag{4}$$

The capacitance value between the upper and bottom plates can be expressed as [5]

$$C = \frac{\varepsilon_0 A}{g_c + \dfrac{t_{\mathrm{Si_3N_4}}}{\varepsilon_{\mathrm{Si_3N_4}}}} \tag{5}$$

where A is the area of the capacitor plate, t_{Si3N4} is the thickness of the Si_3N_4 isolation layer on the bottom plate and ε_{Si3N4} is the dielectric constant of Si_3N_4. The gap between upper and bottom plates g_c could be approximately expressed as [6] due to the lever principle and the neglect of lever deformation.

$$g_c = \frac{l_2}{l_1} \times (g_0 - g) + g_{0c} \qquad [6]$$

To design a variable capacitor with large tuning ratio, low control voltage and initial capacitance value C_{max} more than 2.5pF, the capacitor plate area is designed 200 × 200 μm^2. (The width of the control electrode is also 200μm.) The Thickness of the Si_3N_4 isolation layer, t_{Si3N4}, is 3000Å. The initial gap between the capacitor's upper plate and lower plate, g_{0c}, is 0.1μm. To get a stable structure and a reasonable control voltage, the length, width and thickness of the torsion beam, l_t, w_t and t_t, are 50μm, 25μm and 2μm, respectively. Zero-biased beam height of the outer end of the lever, g_0, is 3μm. Then, the relationship between l_1, l_2 and l_3 will be analyzed and how they affect the linearity of C-V response will be presented. Finally, the optimized parameters will be given. The linearity factor LF can be calculated as [7]

$$LF = \frac{n\sum_{i=0}^{n} C_i V_i - \sum_{i=0}^{n} C_i \sum_{i=0}^{n} V_i}{\sqrt{\left[n\sum_{i=0}^{n} C_i^2 - \left(\sum_{i=0}^{n} C_i\right)^2\right]\left[n\sum_{i=0}^{n} V_i^2 - \left(\sum_{i=0}^{n} V_i\right)^2\right]}} \qquad [7]$$

To analysis how lever ratio $l_1/\ l_2$ affect linearity of C-V response and the capacitance tuning ratio, Figure 4 shows the relationship of gap distance g_c versus control voltage and capacitance versus control voltage with different lever ratio $l_1/\ l_2$. When $l_1/\ l_2$ changes from 1 to 10, the capacitance tuning ratio diminishes as 814%, 671%, 457% and 171%, respectively and the calculated LF values are 98.32%, 98.99%, 99.86% and 96.95%, respectively. The tuning ratio is maximized when $l_1/\ l_2$=1 due to the larger g_c, but the LF value 98.32% does not reach the maximum in this situation. As calculated, the optimized LF value maximizes to be 99.90% when $l_1/\ l_2$ is 1.875 and the capacitance tuning ratio is 470% in this situation.

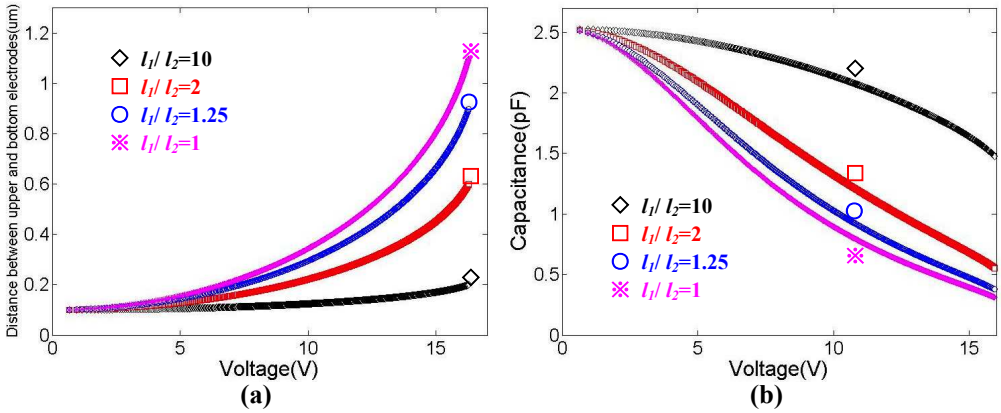

Figure 4. Calculated results of (a) gap distance versus control voltage (b) capacitance versus control voltage when $l_1/\ l_2$ is 1, 1.25, 2 and 10.

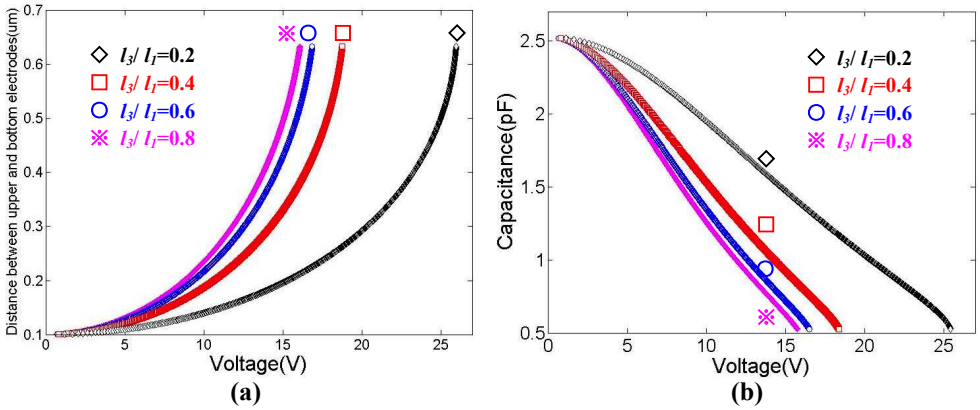

Figure 5. Calculated results of (a) gap distance versus control voltage (b) capacitance versus control voltage when l_3/l_1 is 0.2, 0.4, 0.6 and 0.8.

To analysis how relative length of control electrode l_3/l_1 affect the control voltage and linearity of C-V response, Figure 5 shows the relationship of gap distance versus control voltage and capacitance versus control voltage with different relative length of electrode l_3/l_1 . When l_3/l_1 changes from 0.2 to 0.8, the calculated maximum control voltage needs to be 26.0V, 18.8V, 16.8V and 16.1V, respectively, to achieve a fixed tuning ratio. The *LF* value diminishes as the relative length of control electrode l_3/l_1 increses, which is 99.94%, 99.91%, 99.86% and 99.80%, respectively. This reveals the smaller relative length of control electrode l_3/l_1 offers a higher *LF* value, but also needs a higher control voltage to achieve the same tuning ratio. Considering the design target of low control voltage and the lithography margin in fabrication, the relative length of control electrode l_3/l_1 was set to 0.75 in this work with a tradeoff with linearity. Considering the balance and stability of the whole structure, the l_1, l_2 and l_3 were finally set to 150μm, 80μm and 110μm, respectively. The optimized structure parameters are listed in TABLE 1. The simulated control voltage was 16.3V with the 480% capacitance tuning ratio as shown in Figure 6. The calculated *LF* value was 99.82%.

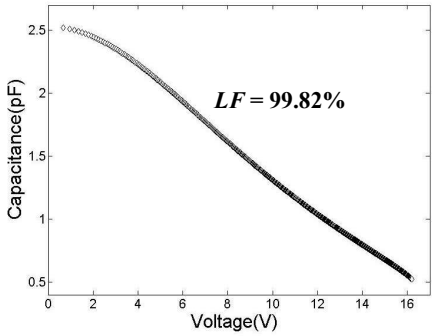

Figure 6. Calculated result of C-V response with optimized structure parameters.

TABLE I. Structure Parameters.

Parameter	Value	Parameter	Value
Area of the capacitor plate (A)	200 × 200 μm^2	Area of control electrode (A_e)	110 × 200 μm^2
Length of the outer end of the lever (l_1)	150μm	Length of the inner end of the lever (l_2)	80μm
Thickness of the upper plate (t)	2μm	Zero-biased beam height of the outer lever (g_0)	3μm

Conclusion

The influence of human body on the communication performance is analyzed. According to the simulation over human tissue at 2.45 GHz, the input impedance of a miniaturized loop antenna changes tremendously, which includes the decrease of real part from 165Ω to 12.2Ω and 14% variation of imaginary part, with the gap between antenna and human tissue increase from 2mm to 10mm. A variable capacitor with symmetric balanced structure is designed to achieve a large capacitance tuning ratio and an remarkable linearity of the C-V response. The proposed RF MEMS variable capacitor was modeled and simulated. The effect of lever ratio and control electrode size on C-V linearity is analyzed. The results show a high linearity factor (LF) of 99.82% in C-V response and a large tuning ratio of 480% in a low actuation voltage range from 0V to 16.3V.

References

1. N. Q. Bolton, Mobile Device RF Front-End TAM Analysis and Forecast, CS Mantech Conf., May 16-19, (2011).
2. K. Sahota, RF front end requirements for 3G and beyond, Ultrasonics Symposium (IUS), p.86,90, 11-14 Oct. (2010).
3. 3GPP Standard TS 25.101 release 11, available online at http://www.3gpp.org/ftp/specs/html-info/25101.htm.
4. Nick Cheng, J.P. Young, Compound Semiconductor Integrated Circuit Symposium (CSICS), p.1,4, 16-19 Oct. (2011).
5. K. Walsh and J. Johnson, 3G/4G Multimode Cellular FrontEnd Challenges, RFMD White Paper.
6. G.M. Rebeiz, IEEE 13th Topical Meeting on Silicon Monolithic Integrated Circuits in RF Systems (SiRF), p.1,2, 21-23 Jan. (2013).
7. K.R. Boyle, Yun Yuan, L.P. Ligthart, *IEEE Trans. on Antennas and Propagation*, 55(2), (2007).
8. T. Alves, B. Poussot, J.-M. Laheurte, *IEEE Trans. on Antennas and Propagation*, 59(4), (2011).
9. S. Fouladi, F. Domingue, N. Zahirovic, R.R. Mansour, IEEE *Trans. on Micro. Theory and Techniques*, 58(4), (2010).
10. G. M. Rebeiz, *RF MEMS Theory, Design, and Technology*, J.Wiley and Sons, (2003).
11. G.M. Rebeiz, K. Entesari, I. Reines, S.-J. Park, M.A. El-Tanani, A. Grichener, A.R. Brown, *Microwave Magazine*, 10(6), (2009).
12. S.P. Natarajan, S.J. Cunningham, A.S. Morris, D.R. DeReus, IEEE 11th Topical Meeting on Silicon Monolithic Integrated Circuits in RF Systems (SiRF), p. 173, Jan. (2011).
13. A. Morris and S. Cunningham, *ECS Transactions*, 53 (3) 255-263 (2013).
14. O. Degani, E. Socher, A. Lipson, T. Leitner, D. J. Setter, S. Kaldor, Y. Nemirovsky, *J. Microelectromech. Syst.*, 7(4), (1998).
15. S. P. Timoshenko and I. N. Goodier, *Theory of Elasticity*, p. 40–46, McGraw-Hill, New York (1970).